A Case for Line-Of-Sight Blockage Detection as a Primitive in Millimeter-Wave Networks

Sanjib Sur, Srihari Nelakuditi
Department of Computer Science and Engineering, University of South Carolina
sur@cse.sc.edu, srihari@sc.edu

***Abstract*—Millimeter-wave is the core technology for current wireless standards to enable multi-Gbps throughput and ultra-low latency connectivity. However, designing reliable mmWave networks that provide high quality of service is challenging because of the extreme sparsity of the mmWave channel and frequent unavailability of the Line-Of-Sight (LOS) path. To this end, we propose a primitive to detect the state of the LOS path across the entire mmWave frequency band in a *frequency-agnostic* manner. The primitive leverages two key observations: under open LOS, the path is correlated between any two mmWave frequencies; and under the blockage, such correlation disappears. Such a primitive allows a mmWave picocell to achieve the latency of handover below sub-millisecond consistently, change its PHY, MAC, and Network layer policies at run-time adaptively, and ensure the link doesn't suffer from outage proactively. We have validated this primitive on three distinct mmWave frequency bands: 24 GHz; 77 GHz; and 122 GHz, and in the future, we propose to extend the validation to several mmWave frequencies, up to 300 GHz. We also discuss the system-level challenges pertaining to design and implementation of such a primitive for a practical, flexible mmWave networking stack.**

***Index Terms*—Millimeter-wave networks, Line-Of-Sight blockage, Frequency-agnostic blockage detection.**

I. Introduction

Millimeter-wave is the core, new technology for current wireless standards and infrastructures, and is the key enabler for applications that demand multiple Gbps throughput and ultra-low latency connectivity [1]. Although most of the millimeter-wave (mmWave) standards and devices operate below 70 GHz today due to price, policy, and performance [2], some of the successes of 5G have triggered significant interests in academia, industry, and government to explore beyond that limit. Significant research investments from programs, like the DARPA's T-MUSIC and the European Union's H2020 promise to not only improve the device performances but also drive down their price substantially. Besides, FCC recently de-regularized 21 GHz bandwidth above 95 GHz spectrum and now allows permission for experimental licenses up to 3 THz. These critical steps and investments will enable new networking, sensing, imaging, and health services and applications beyond what is promised in 5G [2].

Specifically, the recent availability of inexpensive hardware above 100 GHz [3; 4] makes the time ripe for bringing higher-frequency mmWave networks and applications to the masses. This will catalyze our vision of a future network architecture (Figure 1[c]): Extremely high density of inexpensive picocells, each with thousands of beam directions, deployed on indoor and outdoor structures and operating on hundreds of frequency bands, anywhere from 24 to 170 GHz. However, realizing such networks in practice is challenging. At mmWave, the signal power tends to concentrate around the Line-Of-Sight (LOS) path and a few Non-Line-Of-Sight (NLOS) paths from strong reflectors: In practice, the number of such paths is only 2 or 3 [5]–[9]. *Unavailability or misalignment of the dominating paths, especially the LOS, can substantially degrade the mmWave link's quality of service.* MmWave devices can electronically steer beams to track the most dominating path [10]–[13], but the tracking does not guarantee reliable connectivity during the blockage. Besides, there is no scheme that can *determine the LOS path's availability or quality in a scalable, frequency-agnostic manner*.

Early detection of the LOS path's quality and state can enable ultra-reliable, low-latency connectivity and can become a primitive for ubiquitous mmWave networks. This primitive allows a picocell to *proactively* ensure that the link doesn't suffer from an outage, to *consistently* achieve the latency of handover below sub-millisecond, and to *adaptively* change its PHY, MAC, and Network layer policies at run-time, such as determining the aggressiveness of beam tracking, rate adaptation, power adaptation, and traffic shaping. Figures 1(a–c) show a few of the potential applications of such a primitive. In particular, it can enable the five scenarios below:

- The picocell can proactively coordinate among the neighbors to enable a fast handover of data and control flow reliably without incurring additional latencies.
- Fast-moving aerial platforms, such as drones, can adapt their paths dynamically to enable reliable aerial networks.
- City-wide mesh networks can be deployed in a frequency-agnostic manner, and picocells on the mesh can load-balance adaptively without relying on a fixed, central policy.
- These picocells can also route data in a scalable, reliable manner under occasional disruptions, while still achieving sub-millisecond latency consistently.
- Finally, picocells can release licensed spectrum dynamically when LOS is blocked to enable fast spectrum sharing; besides, they can also use unlicensed spectrum to detect the LOS state without using licensed spectrum, thus, saving precious channel resources.

To this end, we propose a LOS state detection primitive (blocked or not); it operates in a frequency-agnostic manner across the entire mmWave frequency band: between 24 GHz

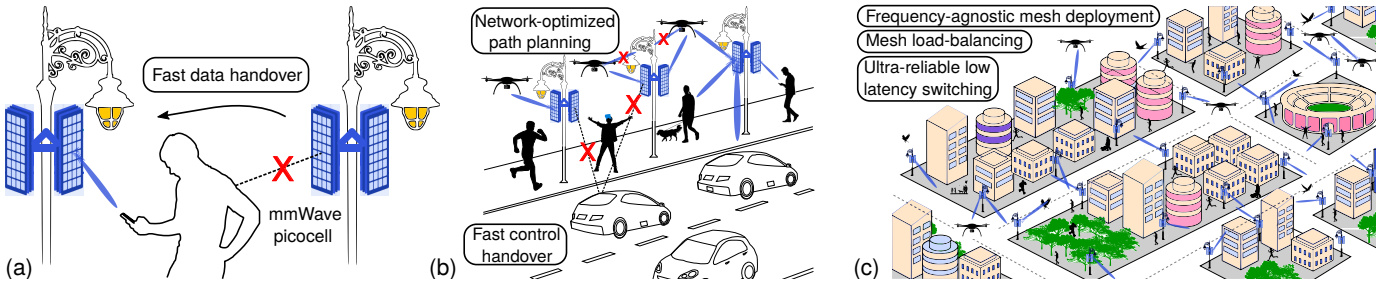

Fig. 1: *A few applications of the LOS state detection: (a) Fast data handover between picocells; (b) Fast control handover for mobile platforms, and network-optimized path planning for aerial platforms; (c) City-wide frequency-agnostic mesh deployment with efficient load-balancing and ultra-reliable, low-latency switching.*

to 300 GHz. The fundamental approach uses two mmWave frequencies, that are far apart from each other, to infer the LOS state of the other mmWave frequencies. Our key idea is intuitive: When the LOS is open between the transmitter and receiver, the difference of the received powers (in dB) between any two mmWave frequencies should follow an almost constant relationship, since the medium is unobstructed. However, under the presence of a blockage on LOS, this difference should vary randomly; this is because the same blocker and NLOS reflectors affect the signal powers of different mmWave frequencies differently [8; 14]–[17].

We have validated this primitive on a small-scale indoor testbed with Commercial-Off-The-Shelf (COTS) platforms operating at three distinct mmWave frequency bands: 24 GHz; 77 GHz; and 122 GHz. In the future, we propose to extend the validation to small and large-scale outdoor settings with several mmWave frequencies, up to 300 GHz. In Section IV, we also discuss the system-level challenges in designing and implementing this primitive.

II. Background and Related Work

Millimeter-Wave Devices and Standards: MmWave devices and standards operate at a very high frequency and wide bandwidth. For example, existing devices for 5G NR and IEEE 802.11ay operate at the frequency ranges between 26.5–29.5 GHz and 57–71 GHz. Specifically, IEEE 802.11ad devices operate on the unlicensed 60 GHz mmWave, and use 2.16 GHz bandwidth to achieve peak bit-rate up to 7 Gbps. Since mmWave channel has a high signal propagation loss, both the standards use phased-array antennas to create electronically steerable beams for signal strength compensation. The small form factor of mmWave radio-frequency components and elements also allows integration of multiple antennas into mobile devices.

Millimeter-Wave Measurements and Modeling: Existing research works have extensively characterized mmWave wireless channels below 90 GHz. The measurements and models identified the effects of distance, environmental reflection, blockage, and statistical properties, such as path loss exponent, delay spread, and angle of arrival distribution [5]–[7; 9; 14; 18]–[21]. Recent works are also looking at the channel characteristics of higher-frequency mmWave: at 140 GHz [15]; between 110–170 GHz [16]; and around 300 GHz [17]. They demonstrate that the LOS power in mmWave channel follows a well-established free-space path loss model. The channel is also extremely sparse, *i.e.*, there exist only a few paths between the transmitter and receiver. Due to such sparsity, mobility and blockage pose grand challenges in designing ultra-reliable mmWave networks.

Millimeter-Wave Link and Network Adaptation: Recent compressed sensing solutions exploit this sparsity of mmWave channel to design scalable beam tracking algorithms [10]; yet they require high computational overhead and may not scale well in practical deployments. Many mmWave systems [11; 12; 22] also explored ways to estimate the beam quality with minimum computation and measurement overheads. But, a fast beam tracking cannot guarantee reliable connectivity to a picocell during the blockage. Moreover, all the existing link and network adaptation algorithms have been validated for mmWave devices operating below 90 GHz [8; 11; 22; 23].

Cross-Frequency Channel Prediction: Prior works, such as [24; 25], used correlation across lower-frequency microwave bands to predict the channel quality without explicit measurement. For example, [24] built a machine learning tool that captures such correlation implicitly and infers the best quality alternative Wi-Fi channel without probing. [25] enabled LTE base stations to infer the downlink channel by measuring the same user's uplink channel. Recently, [26; 27] leveraged the sub-6 GHz channel to narrow down 60 GHz beam tracking space. In contrast, our proposed approach can bring such a prediction across the entire mmWave frequency band and enable a flexible networking stack.

Multiple Radio Interface Collaboration: Existing works on multi-radio collaboration at the microwave bands have focused on four aspects: traffic management [28; 29]; mobility management [30]; energy-efficiency [31; 32]; and routing in multi-band mesh networks [33]–[35]. Also, to enable reliable connectivity and seamless transition from microwave, both 5G NR and IEEE 802.11ad/ay adopted the dual-use of sub-6 GHz and mmWave on user devices and picocells. These standards already specify the MAC-level control and coordination procedures between the picocells and users, to allow the traffic to migrate in between multiple interfaces, and to allow reliability and transparency to higher-layer protocols. Our proposed work is complementary to the existing systems and can benefit from the standardized protocols' evolution.

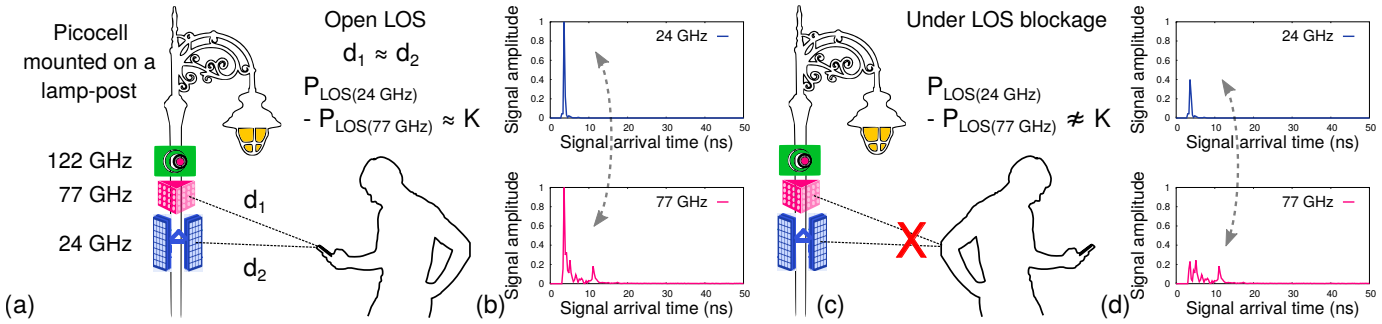

Fig. 2: *Primitive for LOS state detection: (a–b) Under open LOS, received power difference between LOS paths of any two mmWave frequencies follows an almost constant relationship; the picocell tracks this difference continuously; (c–d) Under LOS path blockage, this difference deviates away since the same blockage affects the two frequencies differently.*

III. LOS State Detection Primitive

Our LOS state detection primitive is based on two factors: the past measurement observations that show the same blocker and NLOS reflectors affect the powers of different mmWave frequencies differently [8; 14]–[17]; and our intuition that under an open LOS, the difference of the received powers (in dB) between any two mmWave frequencies follows an almost constant relationship. Figures 2(a–d) show a run-time LOS state detection approach. Imagine a picocell, mounted on a road-side lamp-post, operating at three mmWave frequencies: 24 GHz; 77 GHz; and 122 GHz. When a user is connected to it, the picocell can track the LOS power difference between the currently operational mmWave, say 24 GHz, and one of the other mmWave frequencies, say 77 GHz. Intuitively, under an open LOS, this power difference will remain constant, since the medium is unobstructed. However, when the LOS is blocked, this difference will vary significantly. Based on this variance, the picocell can infer the LOS path's state quickly. We now briefly discuss the rationale behind this intuition.

A. Rationale

Consider two mmWave devices that are d distance apart and are operating at frequency f. Under an open LOS, the received signal power of the LOS path follows the free space model [14]–[17], and is given by:

$$P = k \cdot (\frac{\lambda}{4\pi d})^2 \tag{1}$$

Where λ is the wavelength of the wireless signal ($\lambda = c/f$, $c \approx 3 \times 10^8 m/s$, is the constant speed of wave), and k is the constant gain from three factors: transmit beam; transmit power; and receive beam. If the mmWave devices are transmitting and receiving at two separate frequencies, with wavelengths λ_1 and λ_2, then the corresponding LOS signal powers will be:

$$P_1 = k_1 \cdot (\frac{\lambda_1}{4\pi d_1})^2; \quad P_2 = k_2 \cdot (\frac{\lambda_2}{4\pi d_2})^2; \tag{2}$$

The gain from the transmit beam, transmit power, and receive beam are different for the two frequencies. However, for co-located antennas, the corresponding distances of the LOS for each frequency are almost the same, *i.e.*, $d_1 \approx d_2$. Thus, the ratio of the two LOS powers is given by:

$$\frac{P_1}{P_2} = \frac{k_1}{k_2} \cdot (\frac{\lambda_1}{\lambda_2})^2 \cdot (\frac{d_2}{d_1})^2 \approx \frac{k_1}{k_2} \cdot (\frac{\lambda_1}{\lambda_2})^2$$

Moreover, if the two mmWave frequencies are using a fixed transmit beam, transmit power, and receiver beam, then both k_1 and k_2 remain constant over time. So, the power difference (in dB) between the LOS paths would also remain constant:

$$\begin{aligned} &\textit{Power difference (dB)} = 10log_{10}(P_1) - 10log_{10}(P_2) \\ &= 10log_{10}(\frac{P_1}{P_2}) \approx 10log_{10}(\frac{k_1}{k_2} \cdot (\frac{\lambda_1}{\lambda_2})^2) = \textit{Constant} \end{aligned} \tag{3}$$

However, when the LOS is blocked, the signals no longer follow the free space model since they partially get absorbed, reflected, or refracted by the object in between the transmitter and the receiver. Furthermore, such absorptions, reflections, and refractions are frequency-dependent [8; 14]–[17]. Hence, under the LOS blockage, the power difference in Eq. 3 would fluctuate randomly. Thus, *the presence/absence of LOS blockage can be inferred from the absence/presence of invariance in the power difference*.

B. Measurements

Platforms: To validate this model, we use COTS platforms, from the Texas Instruments and the Silicon Radar GmbH, operating at three distinct mmWave frequencies on the ISM bands: 24 GHz; 77 GHz; and 122 GHz [3; 36]. Figures 3(a–c) show the platforms. All three platforms use phased-array antennas to transmit and receive mmWave signals; besides, the transmitters also use fixed powers below the FCC's limit. The 24 GHz platform operates on a 3.1 GHz channel bandwidth at 23.2–26.3 GHz frequency band, and we fix the center frequency at 23.7 GHz. The 77 GHz platform operates on a 5 GHz channel bandwidth at 76–81 GHz, and we fix the center frequency at 77 GHz. Finally, the 122 GHz platform operates on a 6.8 GHz bandwidth at 119.1–125.9 GHz, and we fix the center frequency at 119.6 GHz. The platforms are designed for radar applications; so they are unable to measure the signal power from distant transmitters. To overcome this limitation, we used a strong metallic reflector in front of the platform; since it reflects back all the signal power without any absorption, it emulates a transmitter. Each phased-array antenna can generate multiple beam directions, but throughout

all our measurements, we use the widest transmit and receive beams. All the mmWave platforms are connected to data capture modules to gather measurements in real-time, and we transfer them via an Ethernet cable to a host laptop for analysis. In order to keep the signal path resolution the same across all three mmWave frequency bands, and in order to be FCC-compliant, we use only 1 GHz bandwidth. This allows all three platforms to resolve the signal paths with 1 ns resolution.

Signal Powers Across LOS and NLOS: To understand the signal power distribution across the LOS and NLOS paths, we measure the mmWave channels at three distinct frequencies but at the same time and space. We set up a receiver 1.8 m. away from a transmitter on a programmable rotating platform (see Figure 4[a]). To measure the signal powers from multiple directions and time, we program the rotating and mmWave platforms to rotate at 2° angular steps and collect measurements across the 1 GHz bandwidth. This setup allows resolving signal power from different paths with 2° space resolution and 1 ns time resolution, sufficient to discriminate all the LOS and NLOS paths.

Figures 4(b–d) show the temporal profiles of the received signal power at 0°, *i.e.*, the receiver pointing directly towards the transmitter. Note that the profile is extremely sparse across all three frequencies, with most of the signal power concentrated in the LOS. Figures 4(e–g) also show the signal power distribution across space; again, the most dominating path is the LOS, and only a few NLOS paths are concentrated around a few directions. Besides, as we move to higher frequencies, the same NLOS reflectors exhibit more roughness because the signal's wavelength is smaller [2]. *These space-time measurements show that the NLOS paths do not have a strong relationship among different frequencies; but, the LOS paths are well-aligned across all three frequencies.*

LOS Relationship Across the mmWave Frequencies: To understand the LOS paths' relationship across the mmWave frequencies, we measure the spatial and temporal profiles at 75 different indoor locations in a home. Both the transmitter and receiver remain static, and the distance between them varies from 1 m. to 10 m. For each of the locations, *first*, we measure the signal power distribution under open LOS. *Then*, we re-measure the distribution by blocking the LOS with random objects and the human body. *Finally*, for each of the scenarios, we calculate the power difference (in dB) between the pair of frequencies: 24 – 77 GHz; 77 – 122 GHz; and 24 – 122 GHz.

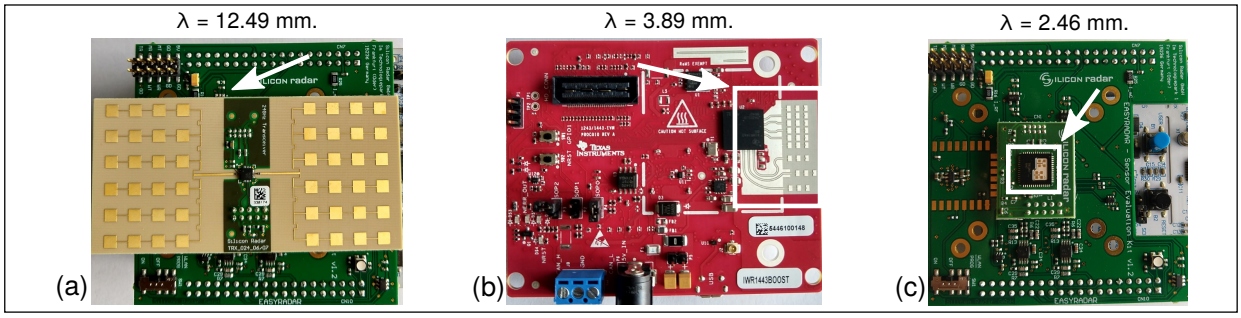

Fig. 3: *Phased-array antennas at three mmWave frequencies: (a) 24 GHz; (b) 77 GHz; and (c) 122 GHz. The wavelength, λ, is shown above: It determines the antenna dimensions.*

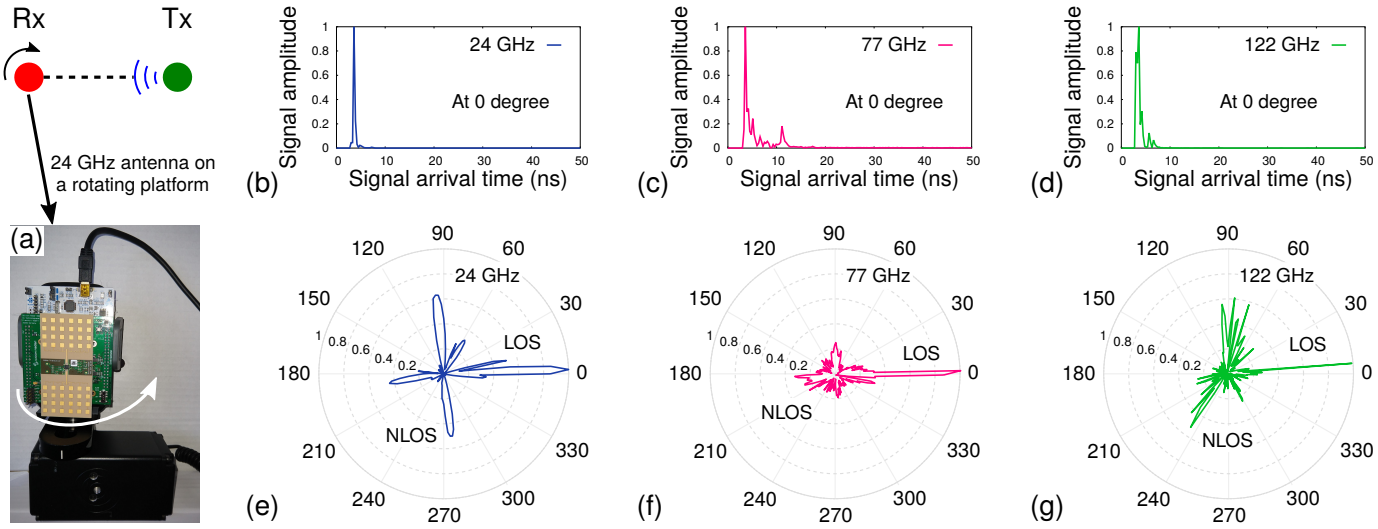

Fig. 4: *(a) Measurement setup: the Rx is placed on a programmable rotating platform; Signal powers in space and time at three mmWave frequencies: 24 GHz; 77 GHz; and 122 GHz. The signal amplitudes are normalized. (b–d) Temporal profiles at 0 degree angle; and (e–g) Spatial profiles. The measurements show that LOS paths are well-aligned and correlated; but, the NLOS paths are not, since the same NLOS reflectors exhibit more roughness at higher frequencies and smaller wavelengths.*

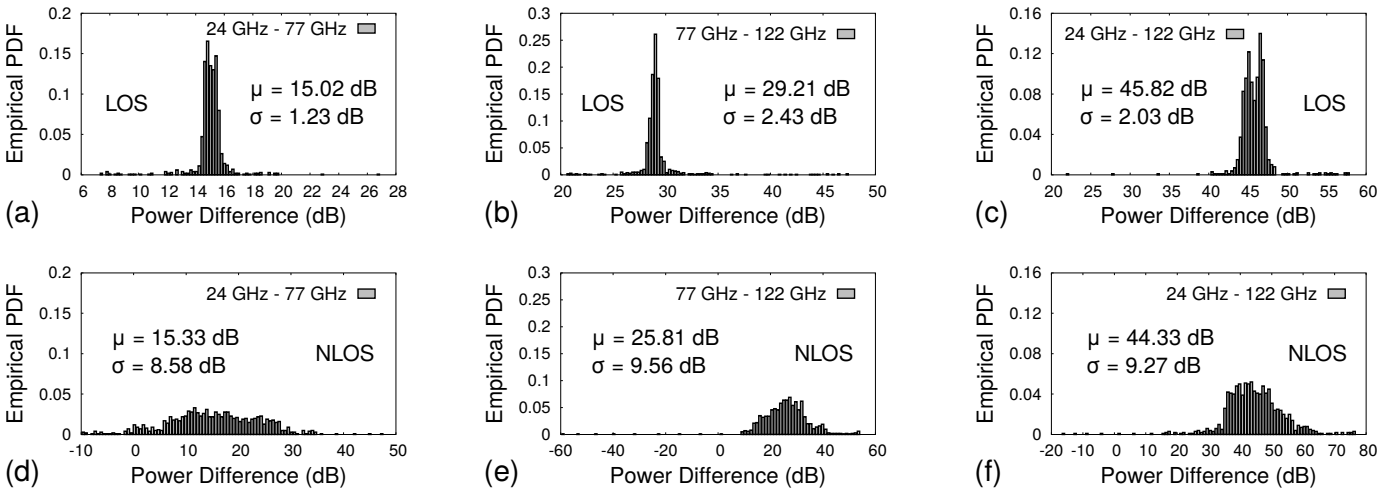

Fig. 5: *Signal power difference of the paths between pair of mmWave frequencies: 24 – 77 GHz; 77 – 122 GHz; and 24 – 122 GHz. (a–c) Under open LOS; and (d–f) When LOS is blocked. The flat distributions under blockage indicate the large variance of the power difference; but, the sharp distributions under open LOS indicate the LOS paths are not only well-aligned but also correlated. So, the LOS path's state can be inferred based on this variance of the power difference.*

Figures 5(a–f) show the aggregated results from all the indoor locations. Each plot shows the empirical probability distribution of the power difference between the pair of mmWave frequencies under open LOS and blocked LOS. When there is an object or human body in between the transmitter and receiver, the power difference varies significantly, indicating that the LOS is blocked. For example, Figure 5(d) shows the power difference between the 24 GHz and 77 GHz when LOS is blocked; it varies from -10 to 47 dB with a mean 15.33 dB and a standard deviation of 8.58 dB. However, Figures 5(a–c) show sharp distribution profiles indicating that when LOS is open, the paths align well, the signal follows the free space, and the power difference follows an almost constant relationship. Thus, *the picocells can infer the LOS path's state based on the power difference variance*.

IV. Practical Challenges

Challenges with Mobile Devices: While it is possible to mount several mmWave radios on a picocell, it may not always be feasible for a mobile device due to constraints from power, circuit area, and price. However, we note that the 5G NR standard already proposes the use of multiple mmWave bands: 26.5 GHz–29.5 GHz; and 37.0 GHz–40.0 GHz. Besides, mmWave WLAN, like IEEE 802.11ad, operates on an unlicensed 57–71 GHz band. Thus, in the future, we can expect mobile devices to be integrated with at least 2 or 3 mmWave radios, and as 5G deployment accelerates and widely gets adopted, the devices' volume productions would drive down the price for multi-radio substantially.

Our primitive assumes that the gains from the transmit beam, transmit power, and receive beam remain constant. This is a valid assumption for a fixed point-to-point mmWave link or mesh network. However, it may not always hold true for mobile devices. In principle, for mobile connectivity, all three parameters can change when the device moves or is far away from the picocell. But we note that such changes are deterministic and are known *a priori* to the picocell. Thus, it can infer the LOS path's state for mobile devices. In the future, we will evaluate this primitive for mobile mmWave devices.

Challenges with Robust State Detection: Our primitive relies on the assumption that the same blocker and NLOS reflectors affect the powers of different mmWave frequencies differently: Prior measurements have shown this assumption's validity at 28, 38, 60, 73 GHz [8; 14], and more recently at 140 GHz, between 110–170 GHz, and around 300 GHz [15]–[17]. Moreover, our experiments in Section III validate the intuition that under open LOS, the difference of the received powers between a pair of mmWave frequencies follow an almost constant relationship. Still, the distribution of power difference in Figures 5(a–c) has a non-zero standard deviation between 1–2.5 dB, *i.e.*, there could be certain cases where such constant relationship may not hold. Such standard deviations occur for various reasons, such as gain fluctuations, noise, *etc.* Thus, the picocell may falsely detect the LOS path's state, which may lead to false triggers of the interface, picocell, or policy change. In the future, we propose to explore a probabilistic state detection primitive in order to be more robust against gain fluctuations and measurement noise.

V. Future Works

Validating LOS State Detection Primitive Extensively: We have validated the detection primitive on the off-the-shelf platforms; yet, the validation is limited to an indoor environment. In the future, we propose to extend the validation to small-scale outdoor settings. Furthermore, we will validate it in a city-wide pedestrian and aerial mmWave testbeds: COSMOS [37] and AERPAW [38]. Besides, we propose to validate the primitive in more mmWave frequencies as more testbeds open up and become accessible to us.

Estimating Quality of LOS Path and Identifying Correlation for NLOS Paths: In practice, mmWave signal power tends to concentrate around 2 or 3 dominating paths: 1 LOS

path, and 1 or 2 NLOS paths. Open LOS paths between any pair of mmWave frequencies are always correlated in strength and direction, and our primitive uses such correlation to detect the state of the LOS path. In the future, we propose to extend the primitive to estimate the quality of the LOS paths of other mmWave frequencies. Moreover, NLOS paths may not be correlated in strength since the objects in the environment show different reflection, diffraction, and absorption properties across different mmWave frequencies. Yet, some of the directions of strong NLOS paths may align well. We propose to leverage this intuition to explore the potential relationship among NLOS paths. This can further open up several avenues of new research directions: from predictable PHY performance at various mmWave frequencies using any arbitrary mmWave band to new modalities of MAC and network layers.

VI. Conclusion

In this work, we propose a primitive to detect the state of the LOS path across the entire mmWave frequency band. The primitive leverages two key observations: under open LOS, the LOS path is correlated between any two mmWave frequencies; and under the blockage, Such primitive could enable high-quality and resilience mmWave networks operating on multiple frequency bands. We use testbed experiments from COTS mmWave devices to demonstrate the validity of the primitive. In the future, we will validate it under several mmWave frequencies, up to 300 GHz, in small and large scale outdoor settings. We will also build on this preliminary work to get a deeper understanding of the correlation properties of LOS and NLOS paths across the entire mmWave spectrum, and to design and implement such a primitive for a practical, flexible mmWave networking stack. Overall, we believe, such a primitive can become a core enabler for ultra-reliable, low-latency, and ubiquitous mmWave networks.

Acknowledgments

This work is partially supported by the NSF under grants CNS-1910853, MRI-2018966, and CAREER-2144505.

References

[1] 3GPP: A Global Initiative, "The Mobile Broadband Standard: Release 17," 2020. [Online]. Available: http://www.3gpp.org/release-17

[2] T. S. Rappaport, Y. Xing, O. Kanhere, S. Ju, A. Madanayake, S. Mandal, A. Alkhateeb, and G. C. Trichopoulos, "Wireless Communications and Applications Above 100 GHz: Opportunities and Challenges for 6G and Beyond," *IEEE Access*, vol. 7, 2019.

[3] Silicon Radar GmbH, "122 GHz Products," 2022. [Online]. Available: https://siliconradar.com/products/#120ghz-radar-chips

[4] Timo Jaeschke, 2022. [Online]. Available: http://www.2pi-labs.com/

[5] M. K. Samimi and T. S. Rappaport, "3-D Statistical Channel Model for Millimeter-Wave Outdoor Mobile Broadband Communications," in *IEEE ICC*, 2015.

[6] T. S. Rappaport, E. Ben-Dor, J. N. Murdock, and Y. Qiao, "38 GHz and 60 GHz Angle-Dependent Propagation for Cellular and Peer-to-Peer Wireless Communications," in *IEEE ICC*, 2012.

[7] H. Xu, V. Kukshya, and T. S. Rappaport, "Spatial and Temporal Characteristics of 60-GHz Indoor Channels," *IEEE JSAC*, vol. 20, 2002.

[8] S. Sur, V. Venkateswaran, X. Zhang, and P. Ramanathan, "60 GHz Indoor Networking through Flexible Beams: A Link-Level Profiling," in *Proc. of ACM SIGMETRICS*, 2015.

[9] P. F. M. Smulders, "Statistical Characterization of 60-GHz Indoor Radio Channels," *IEEE TAP*, vol. 57, no. 10, 2009.

[10] Z. Marzi, D. Ramasamy, and U. Madhow, "Compressive Channel Estimation and Tracking for Large Arrays in mm-Wave Picocells," *IEEE Journal of Selected Topics in Signal Processing*, vol. 10, no. 3, 2016.

[11] H. Hassanieh, O. Abari, M. Rodriguez, M. Abdelghany, D. Katabi, and P. Indyk, "Fast Millimeter Wave Beam Alignment," in *Proc. of ACM SIGCOMM*, 2018.

[12] M. E. Rasekh, Z. Marzi, Y. Zhu, U. Madhow, and H. Zheng, "Noncoherent mmWave Path Tracking," in *ACM HotMobile*, 2017.

[13] T. Wei and X. Zhang, "Pose Information Assisted 60 GHz Networks," in *ACM MobiCom*, 2017.

[14] Y. Azar, G. N. Wong, K. Wang, R. Mayzus, J. K. Schulz, H. Zhao, F. Gutierrez, D. Hwang, and T. S. Rappaport, "28 GHz Propagation Measurements for Outdoor Cellular Communications using Steerable Beam Antennas in New York city," in *IEEE ICC*, 2013.

[15] S. L. H. Nguyen, J. Jarvelainen, A. Karttunen, K. Haneda, and J. Putkonen, "Comparing Radio Propagation Channels Between 28 and 140 GHz Bands in a Shopping Mall," in *EuCAP*, 2018.

[16] S. Kim, W. T. Khan, A. Zajic, and J. Papapolymerou, "D-Band Channel Measurements and Characterization for Indoor Applications," *IEEE Transactions on Antennas and Propagation*, vol. 63, no. 7, 2015.

[17] C.-L. Cheng, S. Kim, and A. Zajic, "Comparison of Path Loss Models for Indoor 30 GHz, 140 GHz, and 300 GHz Channels," in *EuCAP*, 2017.

[18] T. Zwick, T. J. Beukema, and H. Nam, "Wideband Channel Sounder With Measurements and Model for the 60 GHz Indoor Radio Channel," *IEEE TVT*, vol. 54, no. 4, 2005.

[19] H. Xu, T. S. Rappaport, R. J. Boyle, and J. H. Schaffner, "Measurements and Models for 38-GHz Point-to-Multipoint Radiowave Propagation," *IEEE JSAC*, vol. 18, no. 3, 2000.

[20] S. Collonge, G. Zaharia, and G. E. Zein, "Influence of the Human Activity on Wide-Band Characteristics of the 60 GHz Indoor Radio Channel," *IEEE TWC*, vol. 3, no. 6, 2004.

[21] T. A. Thomas, H. C. Nguyen, G. R. M. Jr., and T. S. Rappaport, "3D mmWave Channel Model Proposal," in *IEEE VTC*, 2014.

[22] S. Jog, J. Wang, J. Guan, T. M. H. Hassanieh, and R. R. Choudhury, "Many-to-Many Beam Alignment in Millimeter Wave Networks," in *Proc. of USENIX NSDI*, 2019.

[23] S. K. Saha, S. Aggarwal, R. Pathak, D. Koutsonikolas, and J. Widmer, "MuSher: An Agile Multipath-TCP Scheduler for Dual-Band 802.11ad/ac Wireless LANs," in *Proc. of ACM MobiCom*, 2019.

[24] S. Sen, B. Radunović, J. Lee, and K.-H. Kim, "CSpy: Finding the Best Quality Channel without Probing," in *Proc. of ACM MobiCom*, 2013.

[25] D. Vasisht, S. Kumar, H. Rahul, and D. Katabi, "Eliminating Channel Feedback in Next-Generation Cellular Networks," in *ACM SIGCOMM*, 2016.

[26] T. Nitsche, A. B. Flores, E. W. Knightly, and J. Widmer, "Steering with Eyes Closed: mm-Wave Beam Steering without In-Band Measurement," in *IEEE INFOCOM*, 2015.

[27] N. Gonzalez-Prelcic, A. Ali, V. Va, and R. W. Heath, "Millimeter-Wave Communication with Out-of-Band Information," *IEEE Communications Magazine*, vol. 55, no. 12, 2017.

[28] M. Bennis, M. Simsek, A. Czylwik, W. Saad, S. Valentin, and M. Debbah, "When Cellular Meets WiFi in Wireless Small Cell Networks," *IEEE Communications Magazine*, vol. 51, no. 6, 2013.

[29] R. Mahindra, H. Viswanathan, K. Sundaresan, M. Y. Arslan, and S. Rangarajan, "A Practical Traffic Management System for Integrated LTE-WiFi Networks," in *ACM MobiCom*, 2014.

[30] C. Raiciu, D. Niculescu, M. Bagnulo, and M. J. Handley, "Opportunistic Mobility with Multipath TCP," in *ACM MobiArch*, 2011.

[31] C. Pluntke, L. Eggert, and N. Kiukkonen, "Saving Mobile Device Energy with Multipath TCP," in *ACM MobiArch*, 2011.

[32] I. Pefkianakis, J. Chandrashekar, and H. Lundgren, "User-Driven Idle Energy Save for 802.11x Mobile Devices," in *IEEE MASS*, 2014.

[33] R. Draves, J. Padhye, and B. Zill, "Routing in Multi-Radio, Multi-Hop Wireless Mesh Networks," in *Proc. of ACM MobiCom*, 2004.

[34] M. Alicherry, R. Bhatia, and L. E. Li, "Joint Channel Assignment and Routing for Throughput Optimization in Multiradio Wireless Mesh Networks," *IEEE JSAC*, vol. 24, no. 11, 2006.

[35] A. P. Subramanian, H. Gupta, S. R. Das, and J. Cao, "Minimum Interference Channel Assignment in Multiradio Wireless Mesh Networks," *IEEE Transactions on Mobile Computing*, vol. 7, no. 12, 2008.

[36] Texas Instruments, "IWR1443," 2020. [Online]. Available: https://www.ti.com/tool/IWR1443BOOST

[37] "COSMOS," 2020. [Online]. Available: https://cosmos-lab.org/

[38] "AERPAW," 2020. [Online]. Available: https://aerpaw.org/